

Narrowing the Parameter Space of Collapse Models with Ultracold Layered Force Sensors

A. Vinante^{1,2,*}, M. Carlesso^{3,4}, A. Bassi^{3,4}, A. Chiasera⁵, S. Varas⁵, P. Falferi²,
B. Margesin⁶, R. Mezzena⁷ and H. Ulbricht¹

¹*Department of Physics and Astronomy, University of Southampton, Southampton SO17 1BJ, United Kingdom*

²*INFN-CNR and Fondazione Bruno Kessler, I-38123, Trento, Italy*


³*Department of Physics, University of Trieste, Strada Costiera 11, 34151 Trieste, Italy*

⁴*Istituto Nazionale di Fisica Nucleare, Trieste Section, Via Valerio 2, 34127 Trieste, Italy*

⁵*INFN-CNR CSMFO Lab and FBK Photonics Unit, I-38123 Trento, Italy*

⁶*Fondazione Bruno Kessler—CMM, I-38123, Trento, Italy*

⁷*Department of Physics, University of Trento, I-38123, Trento, Italy*

 (Received 22 February 2020; revised 15 June 2020; accepted 24 July 2020; published 3 September 2020)

Despite the unquestionable empirical success of quantum theory, witnessed by the recent uprising of quantum technologies, the debate on how to reconcile the theory with the macroscopic classical world is still open. Spontaneous collapse models are one of the few testable solutions so far proposed. In particular, the continuous spontaneous localization (CSL) model has become subject of intense experimental research. Experiments looking for the universal force noise predicted by CSL in ultrasensitive mechanical resonators have recently set the strongest unambiguous bounds on CSL. Further improving these experiments by direct reduction of mechanical noise is technically challenging. Here, we implement a recently proposed alternative strategy that aims at enhancing the CSL noise by exploiting a multilayer test mass attached on a high quality factor microcantilever. The test mass is specifically designed to enhance the effect of CSL noise at the characteristic length $r_c = 10^{-7}$ m. The measurements are in good agreement with pure thermal motion for temperatures down to 100 mK. From the absence of excess noise, we infer a new bound on the collapse rate at the characteristic length $r_c = 10^{-7}$ m, which improves over previous mechanical experiments by more than 1 order of magnitude. Our results explicitly challenge a well-motivated region of the CSL parameter space proposed by Adler.

DOI: [10.1103/PhysRevLett.125.100404](https://doi.org/10.1103/PhysRevLett.125.100404)

The question of whether the quantum superposition principle remains valid all the way up to the macroscopic domain is still debated. While the widespread belief is that linearity is a fundamental property of nature [1,2], this assumption has been questioned repeatedly [3–7]. Spontaneous collapse models [8–12] offer a clear and, under fairly general assumptions [13,14], unique phenomenology describing the breakdown of quantum superpositions when moving toward the macroscopic scale, while preserving the quantum properties of microscopic systems. By construction they are empirically falsifiable [15] and are therefore attracting increasing theoretical and experimental interest [16–37].

The general assumption of collapse models is that a universal classical noise drives the state of any material system toward a localized state, even in the absence of any measurement process. An inbuilt amplification mechanism makes sure that the collapse scales with the size of the system, so that only sufficiently macroscopic objects are effectively localized [15].

In this work, we present a new experimental test of the continuous spontaneous localization (CSL) model [9,10].

In CSL, the noise is characterized by two phenomenological parameters: the collapse rate λ , measuring the strength of the collapse, and a characteristic length r_c , defining its spatial resolution. The conservative values $\lambda \simeq 10^{-17} \text{ s}^{-1}$ and $r_c = 10^{-7}$ m [8,9] were initially proposed by Ghirardi *et al.* [8,9] by assuming that the collapse becomes effective at the transition between the mesoscopic and the macroscopic world. A larger value for λ has been suggested by Adler [10] under the assumption that the collapse is already effective at mesoscopic scale, resulting in $\lambda \sim 10^{9\pm 2}$ times larger than at $r_c = 10^{-7}$ m, and $\sim 10^{11\pm 2}$ times larger at $r_c = 10^{-6}$ m. Moreover, according to Adler, much larger or smaller values of r_c are physically less motivated [10].

The current strongest experimental bounds on the CSL parameters come from noninterferometric tests that exploit an unavoidable indirect effect of collapse models, namely a tiny violation of the energy conservation [8]. Relevant examples are spontaneous x-ray emissions from Germanium [18–20], spontaneous heating of massive bulk systems [21–25], or universal force noise on mechanical systems [26–36]. Bounds based on the first two effects are already ruling out Adler’s parameters, but they can be

easily evaded by reasonable assumptions on the spectrum of the CSL noise [21,38]. Conversely, experiments based on mechanical resonators, with characteristic frequency in the mHz–kHz range, are more robust against changes in the noise properties.

In Ref. [31], some of us reported an excess noise in a low temperature cantilever that could be in principle explained by CSL according to Adler’s parameters [10]. Here, we explicitly test this hypothesis by implementing a novel method to significantly enhance, by almost 2 orders of magnitude, the CSL noise, thereby circumventing the intrinsic difficulties of a further direct reduction of thermal and background noise in these experiments. Following Refs. [28–30], the one-sided spectral density of the CSL force noise on the x direction acting on a mass density distribution $\rho(\mathbf{r})$ can be written as

$$S_{F_{\text{CSL}}} = \frac{\hbar^2 \lambda r_c^3}{\pi^{3/2} m_0^2} \int d\mathbf{q} q_x^2 e^{-q^2 r_c^2} |\tilde{\rho}(\mathbf{q})|^2, \quad (1)$$

where $\tilde{\rho}(\mathbf{q})$ is the Fourier transform of $\rho(\mathbf{r})$ and m_0 is the nucleon mass. The effect described by Eq. (1) features a nontrivial dependence on the geometry and can be enhanced around a given r_c by a properly designed multilayered test mass, as discussed in detail in Ref. [39]. In order to detect the smallest possible CSL effect, one needs to minimize the thermal force noise spectral density $S_{F_{\text{th}}} = 4k_B T m \omega_0 / Q$, which calls for mechanical resonators with low temperature T , low frequency ω_0 , and high Q .

In our experiment, the mechanical sensor is a silicon cantilever [see Fig. 1(a)] of the type developed for atomic

force microscopy. The same sensor was used in previous tests of CSL [31]. A multilayer test mass has been glued on the cantilever end [see Fig. 1(b),(c)]. It is a cuboidal structure formed by 47 alternate layers of SiO_2 and WO_3 , fabricated by sputtering. For details on the design and fabrication, see the Supplemental Material [40]. As described in Ref. [39], the multilayer structure enhances the effect of the CSL noise for $r_c \lesssim d/3$ where d is the mean layer thickness. The enhancement scales as the density contrast $\Delta\rho = \rho_1 - \rho_2$ and the number of layers [40]. In this experiment, we have $\rho_1 = 7.17 \times 10^3 \text{ kg/m}^3$ and $\rho_2 = 2.20 \times 10^3 \text{ kg/m}^3$, which are respectively the densities of WO_3 and SiO_2 . The mean layer thickness $d = (370 \pm 4) \text{ nm}$ was specifically chosen to maximize the CSL noise enhancement at $r_c \approx 10^{-7} \text{ m}$. Based on the measured geometrical parameters, we estimate the value of the multilayer mass $m = (7.1 \pm 0.2) \times 10^{-10} \text{ kg}$.

We attach to the cantilever a second smaller mass, a ferromagnetic microsphere, whose motion is detected by a superconducting quantum interference device (SQUID) magnetic flux sensor [see Fig. 1(d)] placed at a distance of $\sim 50 \mu\text{m}$ [31]. This detection method is very convenient and, owing to the low power dissipated by the SQUID, is compatible with the low temperature regime of the experiment. We notice that the ferromagnetic sphere and the cantilever itself give additional, although smaller, contributions to the CSL force noise, which have been accounted for.

The cantilever and SQUID are enclosed in a mechanically isolated shielded copper box thermally linked to the mixing chamber plate of a dry dilution refrigerator. The mixing chamber temperature is stabilized by a proportional integral differential controller. Before performing any measurement, we wait for at least two hours to ensure that the temperature is settled, although the thermalization time is expected to be much shorter. We measure the resonance frequency and quality factor of the fundamental flexural mode of the cantilever by means of ringdown measurements. The resonance frequency is $f_0 = 3532.7 \text{ Hz}$, while it was measured as $f'_0 = 8174 \text{ Hz}$ before attaching the multilayer test mass and with the magnetic sphere already in place [31]. Accordingly, we use the added mass method to estimate the effective stiffness k of the cantilever with respect to the effective position of the test mass on the cantilever. We obtain the value $k = (0.43 \pm 0.01) \text{ N/m}$. As observed in a previous experiment, the intrinsic quality factor depends slightly on temperature [40], likely due to two-level systems in the silicon cantilever [31]. The maximum measured quality factor is $Q = (2.83 \pm 0.03) \times 10^6$ at the lowest operation temperature $T = 30 \text{ mK}$. Remarkably, attaching the large test mass on the cantilever did not spoil the very high Q factor [31]. This result was crucial to keep a very low thermal noise and was achieved through a careful gluing procedure [40]. However, a larger mass implies higher

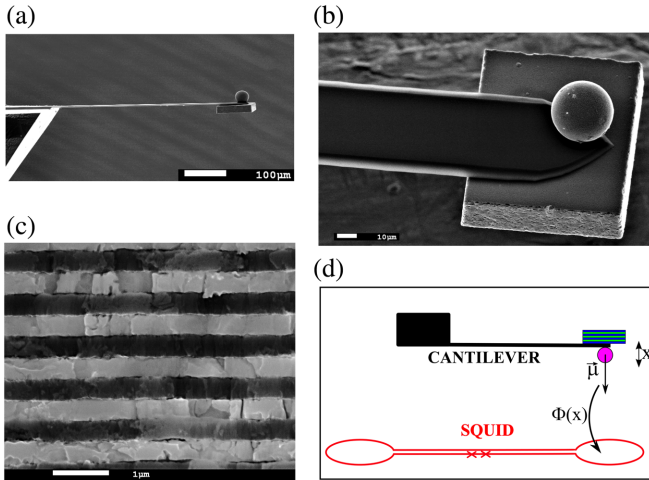


FIG. 1. Details of the experiment. (a) Low resolution SEM micrograph of the assembled cantilever with the multilayer test mass and the magnetic microsphere. (b),(c) SEM micrographs of the multilayer test mass from top (b) and side (c) view, respectively. Here, the alternate layers of WO_3 and SiO_2 are shown in bright and dark, respectively. (d) Simplified scheme of the detection technique, with a gradiometric SQUID magnetometer that detects the variable magnetic field induced by the oscillating ferromagnetic microsphere.

sensitivity to acceleration noise from external vibrations. For this reason, we developed a new three-stage mass-spring suspension, improving the isolation at $f = f_0$ by about 40 dB.

At a given temperature T , we estimate the power spectral density of the force noise by acquiring and averaging a large number of high resolution periodograms of the SQUID magnetic flux signal. The cantilever motion appears as a resonant peak centered at f_0 on top of a white noise floor mainly due to the SQUID imprecision noise. The amplitude of the peak depends on T . Some representative averaged spectra are shown in Fig. 2. We perform a weighted fit of each spectrum with the theoretical curve [40] expressed by

$$S_{\Phi} = A + \frac{Bf_0^4 + C(f^2 - f_1^2)^2}{(f^2 - f_0^2)^2 + (\frac{ff_0}{Q'})^2}. \quad (2)$$

Here, the apparent quality factor Q' takes the place of the intrinsic (or true) Q , which is related to the thermal noise. Q' is generally different from Q due to a well understood cold damping effect induced by the SQUID feedback electronics [31]. The noise parameters A and C and the antiresonance f_1 are related to the SQUID noise operated under a conventional flux-locked loop (i.e., negative feedback) and are almost temperature independent. A full noise model discussing the origin of these terms is discussed in the Supplemental Material [40]. The Lorentzian term amplitude B contains the relevant information on the force noise and can be expressed as

$$B = \Phi_x^2 \left(\frac{S_{F0}}{k^2} + \frac{4k_B T}{k\omega_0 Q} \right), \quad (3)$$

where $\Phi_x = d\Phi/dx$ is the magnetomechanical coupling factor that converts a cantilever displacement x into a SQUID magnetic flux Φ , S_{F0} is the spectral density of any

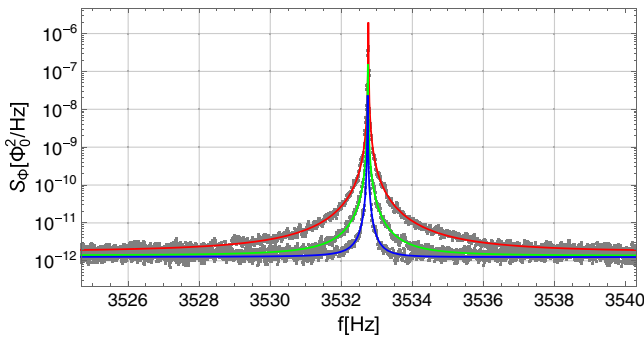


FIG. 2. Representative averaged power spectra of the SQUID flux noise around the cantilever fundamental resonance. The curves refer to the temperatures $T = 1000$ mK, $T = 200$ mK, and $T = 30$ mK, respectively, from the top to the bottom. The solid lines are the best fits to the three datasets with Eq. (2).

nonthermal force noise, and the last term is the thermal noise, which according to the fluctuation-dissipation theorem is proportional to T/Q . The identification of the latter term in Eq. (3) allows us to determine Φ_x and thus to calibrate any nonthermal contribution to B .

Figure 3 shows the measured B as a function of T/Q where $Q = Q(T)$ is measured at the same temperature T . The data follow the expected linear behavior described in Eq. (3) down to $T/Q = 67$ nK, which corresponds to $T = 100$ mK. However, the data at lower temperatures (inset of Fig. 3) indicate a crossover to a different linear regime characterized by a lower slope and positive intercept. This behavior is definitely incompatible with Eq. (3) and in particular cannot be explained by temperature independent noise such as CSL.

A possible explanation is to assume that at least two dissipation channels are acting on the cantilever motion, one of which is not cooling further below the crossover temperature [30,49]. Formally, we split the dissipation as $1/Q = 1/Q_a + 1/Q_b$, where Q_a and Q_b are associated with different thermal baths at the temperatures T_a and T_b , respectively. In the high temperature limit, the system is well thermalized, and $T_a = T_b = T$, where T is the temperature measured by a calibrated thermometer placed on the experimental stage. In the low temperature limit, one of the two temperatures, say T_a , saturates to a constant crossover temperature $T_a \approx T_{co}$, while the second bath is still well thermalized, $T_b = T$.

Thermal saturations in low temperature systems are typically described by the relation

$$T_a = (T_{co}^n + T^n)^{1/n}. \quad (4)$$

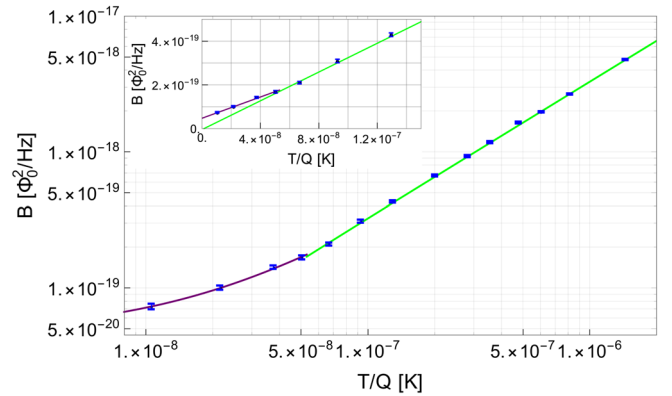


FIG. 3. Measured amplitude of the Lorentzian peak B as function of T/Q . The main panel shows all data in log-log scale for better visualization. The inset reports only the low temperature points in linear scale to underline the crossover between the high temperature and low temperature regimes. The two solid curves represent the linear fits for the points below and above crossover temperature. The linear fit of the data at high temperature is used to bound the CSL noise.

Such a relation is obtained by assuming a steady heat load on the bath at T_a combined with a finite thermal conductance toward the main bath at T , varying as T^{n-1} [49,50]. The most common exponent is $n = 4$ and is related to a contact thermal resistance. In our case, we suspect that the cantilever motion couples magnetically to dissipating elements located on the SQUID chip, which is expected to saturate in the 50–100 mK temperature range. The dissipating elements could be either surface electron spins [51] or vortices in superconducting films [52]. A simple thermal model supporting this possibility is discussed in the Supplemental Material [40]. There, we also fit the whole dataset of Fig. 3 with the combined function $B = B_0 + B_a(x^4 + x_{co}^4)^{1/4} + B_b x$, where $x = T/Q$, while B_0 , B_a , and B_b are fitting constants determining the constant contribution and the thermal noise from baths a and b , respectively. This analysis provides a determination of the crossover at $x_{co} = (T/Q)_{co} \approx 53$ nK, which corresponds to $T_{co} \approx 85$ mK. Note that the saturation is effectively very sharp, so that the related excess noise rapidly vanishes for $T \gtrsim T_{co}$. However, the data of Fig. 3 are in principle compatible with other models with larger n and thus do not allow one to make conclusive claims on the actual saturation mechanism.

In the following, we will make the assumption that the observed crossover is indeed related to a thermal saturation, regardless of its precise physical origin, meaning that for $T < T_{co}$ the data cannot be simply interpreted by Eq. (3). Therefore, to estimate the magnitude of a possible CSL noise effect compatible with the experiment, we restrict our analysis to the range $T \geq 100$ mK. The restricted dataset follows a linear behavior remarkably well. A weighted orthogonal linear fit with the function $B_0 + B_1 T/Q$ yields the values $B_0 = (-4.64 \pm 5.31) \times 10^{-21} \Phi_0^2/\text{Hz}$ and the slope $B_1 = (3.29 \pm 0.03) \times 10^{-12} \Phi_0^2/(\text{K} \cdot \text{Hz})$. The fact that the intercept is compatible with 0 is in full agreement with the fluctuation-dissipation theorem, thus indicating that the system is well thermalized in the restricted high temperature range. According to Eq. (3), the fitting parameters B_0 and B_1 can be used to estimate the residual nonthermal force noise, which reads

$$S_{F_0} = \frac{4k_B k B_0}{\omega_0 B_1}, \quad (5)$$

thus giving $S_{F_0} = (-1.51 \pm 1.77) \times 10^{-36} \text{ N}^2/\text{Hz}$. We use the procedure described in Ref. [53] to determine the upper limit on a strictly positive CSL force noise $S_{F_0, \text{CSL}} \leq 2.07 \times 10^{-36} \text{ N}^2/\text{Hz}$ at the 95% confidence level. Note that, according to the form of Eq. (4), any residual effect of saturation in the high temperature data would increase the noise in such a way as to increase the value of B_0 . Therefore, our estimation of CSL noise should be regarded as conservative.

The corresponding upper bound on λ is derived taking into account the actual geometry and the materials of the whole mechanical resonator, which is composed of the multilayer mass, the magnetic sphere, and the cantilever. The contribution from the multilayer mass is largely dominant at $r_c < 10^{-7}$ m and is responsible for a second minimum of the upper bound at $r_c \approx 10^{-7}$ m [39]. The resulting exclusion plot is shown in Fig. 4. The fluctuations in the upper bound due to the uncertainties in the geometry and density of the different subsystems are of the order of the thickness of the curve in Fig. 4 and cannot be appreciated due to the very compressed logarithmic scale.

The current experiment improves significantly, by almost 2 orders of magnitude, the previous upper bounds from cantilever experiments at the correlation length $r_c = 10^{-7}$ m [31] and by more than 1 order of magnitude the bound from LISA Pathfinder [34]. We are thus substantially challenging the parameter region proposed by Adler [10]. Moreover, the data reveal that the excess noise observed in a previous related experiment [31] is incompatible with a CSL effect for $r_c = 10^{-7}$ m. On the other hand, they do not provide substantial new insight into the origin of that excess noise. Indeed, the absolute value of the excess force noise in the previous experiment, featuring the same cantilever, magnet, and SQUID, is compatible

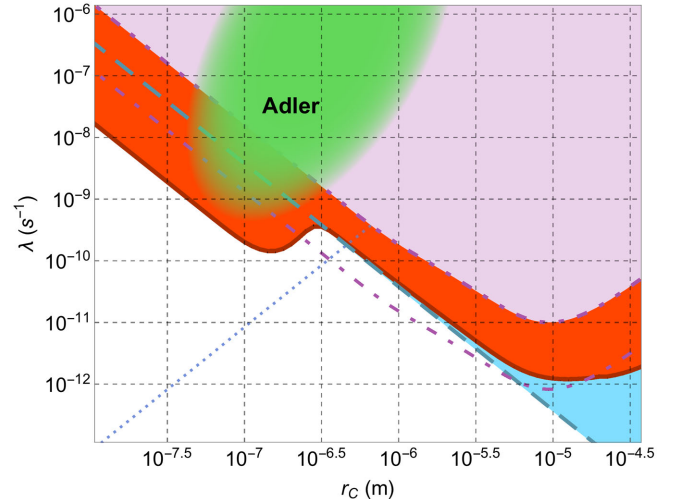


FIG. 4. Exclusion plot for the CSL collapse parameters. Red solid line and shaded area: upper bound and excluded region from the present experiment at the 95% confidence level. Cyan dashed line and shaded area: upper bound and excluded region from LISA Pathfinder [34]. Light purple dash-dot-dotted line and shaded area: upper bound and excluded region from a previous cantilever experiment [31]. Purple dot-dashed line: lower limit of a possible CSL effect from the excess noise observed in the latter experiment [31]. Blue dotted line: upper bound from x-ray emission from a Germanium sample [20]. Since this experiment probes CSL at much higher energies $\sim 10^{19}$ Hz, the upper bound is easily evaded by assuming a spectral cutoff of the CSL noise [38]. The green region represents estimations of CSL parameters from Adler, assuming CSL is effective at mesoscopic scale [10].

with the error bar of the new experiment. The improved bound on the CSL parameters arises entirely from the largest mass load and the specific multilayer structure.

We underline that the strong improvement of the bound at $r_c = 10^{-7}$ m depends on the peculiar features of the CSL model, which make the force noise sensitive to spatial variations of the test mass internal density [39,54]. Different localization models may lead to different behavior. For instance, in the Diosi-Penrose model, the force noise is essentially insensitive to the shape and the spatial distribution of the mass [28,29]. In principle, specific *ad hoc* modifications of the CSL model may lead to a different behavior as well.

Another point to consider here is that the original estimation of the value of λ by Adler was based on very crude assumptions and analysis. Thus, the proposed parameter space represented by the blue region in Fig. 4 should be taken as indicative [55]. In this sense, a further improvement by at least 1 order of magnitude, possibly with different experimental techniques, may be needed to provide a strong falsification of CSL under Adler's assumptions.

Despite these caveats, our measurements are clearly reducing the probability that CSL effects will be found at $\lambda \gtrsim 10^{-10}$ Hz. Eventually, one should explore the more conservative framework initially proposed by Ghirardi *et al.* [9]. In this case, the CSL effects, if existing, could feature a much lower collapse rate λ . Cantilever experiments may be still improved by 1 to 2 orders of magnitude with technological advances in mechanical isolation [56] and a careful characterization of all noise sources. Novel experimental techniques will be needed to fully probe the entire CSL parameter space. Nanomechanical systems at high frequencies [57] and levitated microparticles at low frequencies [35,58–60] are the most promising routes toward this ambitious goal, together with interferometric techniques on earth [17] and in space [61].

The data supporting this study are openly available at Ref. [62].

We gratefully thank S. L. Adler for many stimulating discussions, and N. Bazzanella for technical help. A. B. acknowledges hospitality from the Institute for Advanced Study, Princeton, where part of this work was done. We acknowledge financial support from the EU H2020 FET project TEQ (Grant No. 766900), the Leverhulme Trust (RPG-2016-046), the COST Action QTSpace (CA15220), INFN, and the Foundational Questions Institute (FQXi).

*Corresponding author.

andrea.vinante@ifn.cnr.it

- [1] H. D. Zeh, On the interpretation of measurement in quantum theory, *Found. Phys.* **1**, 69 (1970).
- [2] W. H. Zurek, Decoherence and the transition from quantum to classical, *Phys. Today* **44**, No. 10, 36 (2003).

- [3] E. Schrödinger, Die gegenwärtige Situation in der Quantenmechanik, *Die Naturwissenschaften* **23**, 807 (1935).
- [4] J. S. Bell, *Speakable and Unsayable in Quantum Mechanics: Collected Papers on Quantum Philosophy* (Cambridge University Press, Cambridge, England, 1987).
- [5] S. Weinberg, Collapse of the state vector, *Phys. Rev. A* **85**, 062116 (2012).
- [6] A. J. Leggett, Testing the limits of quantum mechanics: Motivation, state of play, prospects, *J. Phys. Condens. Matter* **14**, R415 (2002).
- [7] M. Arndt and K. Hornberger, Testing the limits of quantum mechanical superpositions, *Nat. Phys.* **10**, 271 (2014).
- [8] G. C. Ghirardi, A. Rimini, and T. Weber, Unified dynamics for microscopic and macroscopic systems, *Phys. Rev. D* **34**, 470 (1986).
- [9] G. C. Ghirardi, P. Pearle, and A. Rimini, Markov processes in Hilbert space and continuous spontaneous localization of systems of identical particles, *Phys. Rev. A* **42**, 78 (1990).
- [10] S. L. Adler, Lower and upper bounds on CSL parameters from latent image formation and IGM heating, *J. Phys. A* **40**, 2935 (2007).
- [11] L. Diosi, Models for universal reduction of macroscopic quantum fluctuations, *Phys. Rev. A* **40**, 1165 (1989).
- [12] R. Penrose, On gravity's role in quantum state reduction, *Gen. Relativ. Gravit.* **28**, 581 (1996).
- [13] N. Gisin, Stochastic quantum dynamics and relativity, *Helv. Phys. Acta* **62**, 363 (1989).
- [14] N. Gisin, Weinberg's non-linear quantum mechanics and supraluminal communications, *Phys. Lett.* **143A**, 1 (1990).
- [15] A. Bassi, K. Lochan, S. Satin, T. P. Singh, and H. Ulbricht, Models of wave-function collapse, underlying theories, and experimental tests, *Rev. Mod. Phys.* **85**, 471 (2013).
- [16] K. Hornberger, S. Gerlich, P. Haslinger, S. Nimmrichter, and M. Arndt, Quantum interference of clusters and molecules, *Rev. Mod. Phys.* **84**, 157 (2012).
- [17] Y. Y. Fein, P. Geyer, P. Zwick, F. Kiaka, S. Pedalino, M. Mayor, S. Gerlich, and M. Arndt, Quantum superposition of molecules beyond 25 kDa, *Nat. Phys.* **15**, 1242 (2019).
- [18] C. Curceanu, B. C. Hiesmayr, and K. Piscicchia, X-rays help to unfuzzy the concept of measurement, *J. Adv. Phys.* **4**, 263 (2015).
- [19] C. Curceanu *et al.*, Spontaneously emitted X-rays: An experimental signature of the dynamical reduction models, *Found. Phys.* **46**, 263 (2016).
- [20] K. Piscicchia, A. Bassi, C. Curceanu, R. D. Grande, S. Donadi, B. C. Hiesmayr, and A. Pichler, CSL collapse model mapped with the spontaneous radiation, *Entropy* **19**, 319 (2017).
- [21] S. L. Adler and A. Vinante, Bulk heating effects as tests for collapse models, *Phys. Rev. A* **97**, 052119 (2018).
- [22] M. Bahrami, Testing collapse models by a thermometer, *Phys. Rev. A* **97**, 052118 (2018).
- [23] R. Mishra, A. Vinante, and T. P. Singh, Testing spontaneous collapse through bulk heating experiments: An estimate of the background noise, *Phys. Rev. D* **98**, 052121 (2018).
- [24] S. L. Adler, A. Bassi, M. Carlesso, and A. Vinante, Testing continuous spontaneous localization with Fermi liquids, *Phys. Rev. A* **99**, 103001 (2019).
- [25] A. Tilloy and T. M. Stace, Neutron Star Heating Constraints on Wave-Function Collapse Models, *Phys. Rev. Lett.* **123**, 080402 (2019).

- [26] B. Collett and P. Pearle, Wavefunction collapse and random walk, *Found. Phys.* **33**, 1495 (2003).
- [27] S. L. Adler, Stochastic collapse and decoherence of a non-dissipative forced harmonic oscillator, *J. Phys. A* **38**, 2729 (2005).
- [28] S. Nimmrichter, K. Hornberger, and K. Hammerer, Optomechanical Sensing of Spontaneous Wave-Function Collapse, *Phys. Rev. Lett.* **113**, 020405 (2014).
- [29] L. Diosi, Testing Spontaneous Wave-Function Collapse Models on Classical Mechanical Oscillators, *Phys. Rev. Lett.* **114**, 050403 (2015).
- [30] A. Vinante, M. Bahrani, A. Bassi, O. Usenko, G. Wijts, and T. H. Oosterkamp, Upper Bounds on Spontaneous Wave-Function Collapse Models Using Millikelvin-Cooled Nanocantilevers, *Phys. Rev. Lett.* **116**, 090402 (2016).
- [31] A. Vinante, R. Mezzena, P. Falferi, M. Carlesso, and A. Bassi, Improved Noninterferometric Test of Collapse Models Using Ultracold Cantilevers, *Phys. Rev. Lett.* **119**, 110401 (2017).
- [32] M. Carlesso, A. Bassi, P. Falferi, and A. Vinante, Experimental bounds on collapse models from gravitational wave detectors, *Phys. Rev. D* **94**, 124036 (2016).
- [33] B. Helou, B. Slagmolen, D. E. McClelland, and Y. Chen, LISA pathfinder appreciably constrains collapse models, *Phys. Rev. D* **95**, 084054 (2017).
- [34] M. Carlesso, M. Paternostro, H. Ulbricht, A. Vinante, and A. Bassi, Non-interferometric test of the continuous spontaneous localization model based on rotational optomechanics, *New J. Phys.* **20**, 083022 (2018).
- [35] D. Zheng *et al.*, Room temperature test of wave-function collapse using a levitated micro-oscillator, *Phys. Rev. Research* **2**, 013057 (2020).
- [36] K. Komori, Y. Enomoto, C. P. Ooi, Y. Miyazaki, N. Matsumoto, V. Sudhir, Y. Michimura, and M. Ando, Attonewton-meter torque sensing with a macroscopic optomechanical torsion pendulum, *Phys. Rev. A* **101**, 011802(R) (2020).
- [37] M. Bilardello, S. Donadi, A. Vinante, and A. Bassi, Bounds on collapse models from cold-atom experiments, *Phys. A* **462**, 764 (2016).
- [38] M. Carlesso, L. Ferialdi, and A. Bassi, Colored collapse models from the non-interferometric perspective, *Eur. Phys. J. D* **72**, 159 (2018).
- [39] M. Carlesso, A. Vinante, and A. Bassi, Multilayer test masses to enhance the collapse noise, *Phys. Rev. A* **98**, 022122 (2018).
- [40] See Supplemental Material at <http://link.aps.org/supplemental/10.1103/PhysRevLett.125.100404> for additional details on fabrication, modeling and data analysis, which includes Refs. [41–48].
- [41] A. Chiasera, C. Meroni, F. Scotognella, Y. G. Boucher, G. Galzerano, A. Lukowiak, D. Ristic, G. Speranza, S. Valligatla, S. Varas, L. Zur, M. Ivanda, G. C. Righini, S. Taccheo, R. Ramponi, and M. Ferrari, Coherent emission from fully Er³⁺ doped monolithic 1-D dielectric microcavity fabricated by rf-sputtering, *Opt. Mater.* **87**, 107 (2019).
- [42] M. Ketchen *et al.*, Octagonal washer DC SQUIDs and integrated susceptometers fabricated in a planarized sub- μm Nb-AlO_x-Nb technology, *IEEE Trans. Appl. Supercond.* **3**, 1795 (1993).
- [43] C. Hilbert and J. Clarke, Measurements of the dynamic input impedance of a dc SQUID, *J. Low Temp. Phys.* **61**, 237 (1985).
- [44] C. D. Tesche and J. Clarke, dc SQUID: Current noise, *J. Low Temp. Phys.* **37**, 397 (1979).
- [45] P. Falferi, M. Bonaldi, M. Cerdonio, R. Mezzena, G. A. Prodi, A. Vinante, and S. Vitale, 10 \hbar superconducting quantum interference device amplifier for acoustic gravitational wave detectors, *Appl. Phys. Lett.* **93**, 172506 (2008).
- [46] D. Freedman and P. Z. Diaconis, On the histogram as a density estimator: L2 theory, *Wahrscheinlichkeitstheorie Verw. Gebiete* **57**, 453 (1981).
- [47] F. C. Wellstood, C. Urbina, and J. Clarke, Hot-electron effects in metals, *Phys. Rev. B* **49**, 5942 (1994).
- [48] A. Vinante, P. Falferi, R. Mezzena, and M. Mück, Hot-electron effect in palladium thin films, *Phys. Rev. B* **75**, 104303 (2007).
- [49] O. Usenko, A. Vinante, G. Wijts, and T. H. Oosterkamp, A superconducting quantum interference device based read-out of a subattonewton force sensor operating at millikelvin temperatures, *Appl. Phys. Lett.* **98**, 133105 (2011).
- [50] F. Pobell, *Matter and Methods at Low Temperatures*, 3rd ed. (Springer, Berlin, 2002).
- [51] A. Vinante, G. Wijts, O. Usenko, L. Schinkelshoek, and T. H. Oosterkamp, Magnetic resonance force microscopy of paramagnetic electron spins at millikelvin temperatures, *Nat. Commun.* **2**, 572 (2011).
- [52] G. Stan, S. B. Field, and J. M. Martinis, Critical Field for Complete Vortex Expulsion from Narrow Superconducting Strips, *Phys. Rev. Lett.* **92**, 097003 (2004).
- [53] G. J. Feldman and R. D. Cousins, Unified approach to the classical statistical analysis of small signals, *Phys. Rev. D* **57**, 3873 (1998).
- [54] L. Diosi, Two invariant surface-tensors determine CSL of massive body wave function, [arXiv:1908.02195](https://arxiv.org/abs/1908.02195).
- [55] S. L. Adler (private communication).
- [56] M. de Wit, G. Welker, K. Heeck, F. M. Buters, H. J. Eerkens, G. Koning, H. van der Meer, D. Bouwmeester, and T. H. Oosterkamp, Vibration isolation with high thermal conductance for a cryogen-free dilution refrigerator, *Rev. Sci. Instrum.* **90**, 015112 (2019).
- [57] S. Forstner, M. Zych, S. Basiri-Esfahani, K. E. Khosla, and W. P. Bowen, Nanomechanical test of quantum linearity, [arXiv:1909.01608](https://arxiv.org/abs/1909.01608).
- [58] A. Vinante, A. Pontin, M. Rashid, M. Toroš, P. R. Barker, and H. Ulbricht, Testing collapse models with levitated nanoparticles: Detection challenge, *Phys. Rev. A* **100**, 012119 (2019).
- [59] B. R. Slezak, C. W. Lewandowski, J.-F. Hsu, and B. D’Urso, Cooling the motion of a silica microsphere in a magneto-gravitational trap in ultra-high vacuum, *New J. Phys.* **20**, 063028 (2018).
- [60] A. Vinante, P. Falferi, A. Setter, C. Timberlake, and H. Ulbricht, Ultralow Mechanical Damping with Meissner-Levitated Ferromagnetic Microparticles, *Phys. Rev. Applied* **13**, 064027 (2020).
- [61] R. Kaltenbaek *et al.*, Macroscopic Quantum Resonators (MAQRO): 2015 update, *Eur. Phys. J. Quantum Technol.* **3**, 5 (2016).
- [62] <https://doi.org/10.5258/SOTON/D1500>.